

# Wide-field Infrared Survey Explorer (WISE)

## Subsystem Design Specification: Multiband DETector (MDET)

Version 2.0

January 12, 2009

Prepared by: Ken Marsh



Infrared Processing and Analysis Center  
California Institute of Technology

WSDC D-D004

**Concurred By:**

---

Roc Cutri, WISE Science Data Center Manager

---

Tim Conrow, WISE Science Data Center Lead Architect

---

Ken Marsh, WISE Science Data Center Cognizant Engineer/Scientist

## Revision History

<b>Date</b>	<b>Version</b>	<b>Author</b>	<b>Description</b>
11/30/07	1.0	Ken Marsh	Initial Draft
1/22/08	1.1	Ken Marsh	1st revision
1/12/09	2.0	Ken Marsh	2nd revision

# Contents

<b>1</b>	<b>INTRODUCTION</b>	<b>5</b>
1.1	Document Scope . . . . .	5
1.2	Applicable Documents . . . . .	5
1.3	Requirements . . . . .	5
1.4	Acronyms . . . . .	6
<b>2</b>	<b>OVERVIEW OF APPROACH</b>	<b>6</b>
<b>3</b>	<b>THEORETICAL BASIS</b>	<b>7</b>
3.1	Measurement Model . . . . .	7
3.2	Detection Algorithm . . . . .	8
3.3	The Effect of Cross-Band Source Blending . . . . .	10
<b>4</b>	<b>IMPLEMENTATION</b>	<b>11</b>
4.1	Procedure . . . . .	11
4.2	Allowance for confusion . . . . .	14
4.3	Inputs . . . . .	16
4.4	Outputs . . . . .	16
<b>5</b>	<b>TESTING</b>	<b>18</b>
<b>6</b>	<b>REMAINING ISSUES</b>	<b>19</b>
<b>7</b>	<b>SUMMARY</b>	<b>19</b>
<b>8</b>	<b>ACKNOWLEDGEMENTS</b>	<b>19</b>
<b>9</b>	<b>REFERENCES</b>	<b>20</b>

# 1 INTRODUCTION

## 1.1 Document Scope

This Subsystem Design Specification (SDS) document describes the design of the Multiband DETection module (MDET) for the WISE Science Data System (WSDS). The purpose of MDET is to produce a list of source candidates in a given region of the sky as the first of two principal steps in the source extraction process. The second step, namely source characterization, will be carried out using the WPHOT module to be described in a separate document.

## 1.2 Applicable Documents

This plan conforms to the specifications in the following project documents:

1. WISE Science Data System (WSDS) Functional Requirements Document (WSDC D-R001).
2. WSDS Functional Design Document (WSDC D-D001).
3. AWAIC Subsystem Design Specification (WSDC D-D005).
4. Software Interface Specification for call to MDET.
5. Software Interface Specification for output to WPHOT.

## 1.3 Requirements

The following requirements (from the WSDC Functional Requirements Document) are relevant to the design of MDET:

- L4WSDC-002*: The WSDC shall produce a Source Catalog derived from the images used to generate the WISE digital Image Atlas.
- L4WSDC-080*: The final WISE Source Catalog shall have greater than 99.9% reliability for sources detected in at least one band with  $\text{SNR} > 20$ , where the noise includes flux errors due to zodiacal foreground emission, instrumental effects, source photon statistics, and neighboring sources. This requirement shall not apply to sources that are superimposed on an identified artifact.
- L4WSDC-009*: The final WISE Source Catalog shall be at least 95% complete for sources detected with  $\text{SNR} > 20$  in at least one band, where the noise includes flux errors due to zodiacal foreground emission, instrumental effects, source photon statistics, and neighboring sources. This requirement shall not apply to sources that are superimposed on an identified artifact.

*L4WSDC-010*: The final WISE Source Catalog shall include sources down to SNR=5 in any band, and the completeness and reliability of sources in the Catalog shall be characterized at all flux levels.

*L4WSDC-043*: The WSDS Pipeline processing shall detect sources down to a threshold of at least five times the image noise from the calibrated image frames, and the combined Atlas Images.

*L4WSDC-044*: The WSDS Pipeline processing shall merge source detections in the four WISE bands into a single source catalog entry.

*L4WSDC-049*: The WSDS Pipeline shall be robust to data missing from one or more bands.

## 1.4 Acronyms

**AWAIC** – A Wise Astronomical Image Coadder; the name of the module used to combine a set of focal-plane images to produce an estimate of the intensity distribution on the sky.

**FITS** – Flexible Image Transport System.

**FWHM** – Full Width at Half Maximum.

**MDET** – Multiband DETector; the name of the module, described here, whose purpose is to produce a list of candidate source detections.

**PSF** – Point Spread Function, defined here as the response of a focal plane pixel to a point source, as a function of position on the sky.

**SNR** – Signal to noise ratio, defined here as the ratio of peak detection signal to the standard deviation of additive noise.

**WCS** – World Coordinate System.

**WPHOT** – WISE PHOTometry module, which will enable both aperture and profile-fitting photometry based on the list of candidates supplied by MDET.

**WSDS** – WISE Science Data System.

## 2 OVERVIEW OF APPROACH

MDET is designed to perform the source detection step associated with each of the three stages of source extraction during pipeline processing (single-frame, single-epoch 4-band frameset, and final coadd stage). With the exception of the single-frame stage (used for frame position reconstruction only), the detection is done at multiple bands simultaneously. It is based on the thresholding of a “detection” image derived from a set of matched filter images in the relevant bands. This detection step will be followed

by a source characterization step using WPHOT which will include the capability of simultaneous multiband photometry using the maximum likelihood (profile-fitting) procedure.

The advantages of doing the detection simultaneously at multiple bands are:

1. Increased sensitivity to weak sources due to the fact that detection is based on the stack of images at all bands.
2. No separate bandmerging step is required, thus avoiding the ambiguities which can occur when trying to associate sources in different bands in the presence of confusion.
3. The higher resolution data at the shorter wavelengths can guide the extraction at the longer wavelengths where the resolution is poorer.

The multiband estimation process represents a departure from the traditional procedure, employed in such software packages as DAOPHOT (Stetson 1987) and SExtractor (Bertin & Arnouts 1996), in which detection and characterization are carried out one band at a time. Another motivation for developing new source extraction algorithms is that currently available packages operate on a single regularly-sampled image rather than a set of dithered images. The procedures employed in MDET (and planned for WPHOT) are optimized for the latter case. MDET is based on an algorithm which is optimal for the detection of non-blended point sources in the presence of additive Gaussian noise, given an observed image or a set of observed images (spatially dithered and/or at one or more bands). Some implications of the “non-blended” assumption will be discussed in Section 4.3.

Inputs to MDET include the coadded images and their uncertainties, generated by the AWAIC module, and a detection threshold representing the assumed lower cutoff in signal to noise ratio. The output is a set of source candidates, with equatorial positions, listed in order of decreasing signal to noise ratio. Note that although coadded images are used as input, they are used in such a way that the result is numerically identical to what would have been produced by optimally combining the dithered focal-plane images themselves.

### 3 THEORETICAL BASIS

#### 3.1 Measurement Model

The starting point for the detection step is the measurement model for an isolated point source, assumed to be at location  $\mathbf{s}$  and to have flux  $f_\lambda$  in the waveband denoted by index  $\lambda$ ; it can be expressed as:

$$\rho_{\lambda i} = f_\lambda H_\lambda(\mathbf{r}_{\lambda i} - \mathbf{s}) + b_{\lambda i} + \nu_{\lambda i} \tag{1}$$

where  $\rho_{\lambda i}$  is the observed value of the  $i$ th pixel at sky location  $\mathbf{r}_{\lambda i}$ ,  $H_\lambda(\mathbf{r})$  is the point spread function (PSF) representing the response of a focal-plane pixel to a point

source,  $b_{\lambda i}$  is the background, and  $\nu_{\lambda i}$  is the noise, assumed to be a spatially and spectrally uncorrelated zero-mean Gaussian random process with variance  $\sigma_{\lambda i}^2$ .

It will be advantageous to estimate the background,  $b_{\lambda i}$  ahead of time (using, for example, median filtering with a window size appropriate to the characteristic spatial scale of background variations) and subtract its contribution, so that the measurement model may be rewritten:

$$\rho_{\lambda i} = f_{\lambda} H_{\lambda}(\mathbf{r}_{\lambda i} - \mathbf{s}) + \nu_{\lambda i} \quad (2)$$

### 3.2 Detection Algorithm

Based on the measurement model expressed by Equation (2), the source detection procedure involves comparing the relative probabilities of the following two hypotheses at each location,  $\mathbf{s}$ , within a predefined regular grid of points on the sky:

Hypothesis (A):  $\mathbf{s}$  lies on blank sky at all wavelengths

Hypothesis (B):  $\mathbf{s}$  represents the location of a source whose flux densities are the most probable values, denoted by  $\hat{f}_{\lambda}$ .

To compare these hypotheses requires knowledge of  $\hat{f}_{\lambda}$ , which we obtain by maximizing the conditional probability,  $P(\mathbf{f}|\rho)$ , with respect to  $\mathbf{f}$ , where  $\mathbf{f}$  is a vector whose components are the set of  $f_{\lambda}$ , and  $\rho$  is a vector whose components are the set of pixel values,  $\rho_{\lambda i}$ , in the vicinity of  $\mathbf{s}$ . The conditional probability itself is given by Bayes' rule, i.e.,

$$P(\mathbf{f}|\rho) = P(\rho|\mathbf{f})P(\mathbf{f})/P(\rho) \quad (3)$$

where

$$\ln P(\rho|\mathbf{f}) = -\frac{1}{2} \sum_{\lambda, i} \frac{1}{\sigma_{\lambda i}^2} [\rho_{\lambda i} - f_{\lambda} H_{\lambda}(\mathbf{r}_{\lambda i} - \mathbf{s})]^2 \quad (4)$$

and  $P(\mathbf{f})$  represents our *a priori* knowledge about possible flux values. Our most important piece of knowledge in that regard is that flux is positive. With the exception of the positivity, however, we will assume that we have no prior knowledge of flux or the spectral variation of flux, in order to avoid introducing any color biases in the source detector. We can thus express  $P(\mathbf{f})$  as:

$$P(\mathbf{f}) = \begin{cases} \text{const.} & \text{if } f_{\lambda} \geq 0 \quad \forall \lambda \\ 0 & \text{otherwise} \end{cases} \quad (5)$$

The remaining quantity,  $P(\rho)$ , in (3), represents a normalization factor. The maximization of  $P(\mathbf{f}|\rho)$  then yields:

$$\hat{f}_{\lambda} = 1 \left( \left[ \sum_i \frac{1}{\sigma_{\lambda i}^2} H_{\lambda i} \rho_{\lambda i} \right] / \sum_i \frac{1}{\sigma_{\lambda i}^2} H_{\lambda i}^2 \right) \quad (6)$$

where  $H_{\lambda i} \equiv H_{\lambda}(\mathbf{r}_{\lambda i} - \mathbf{s})$  and  $1(x)$  represents the unit step function, equal to 1 if its argument is nonnegative and 0 otherwise. The summations in (6) are over all pixels within a predefined neighborhood of  $\mathbf{s}$ .

With a further application of Bayes' rule, we can now express the probabilities of hypotheses (A) and (B), above, as:

$$P(\text{sky}|\rho, m_0) = P(\text{sky}, m_0) \prod_{\lambda} P(\rho_{\lambda}|\text{sky}, m_0)/P(\rho_{\lambda}, m_0) \quad (7)$$

$$P(\hat{\mathbf{f}}|\rho, m) = P(\hat{\mathbf{f}}, m) \prod_{\lambda} P(\rho_{\lambda}|\hat{\mathbf{f}}, m)/P(\rho_{\lambda}, m) \quad (8)$$

where  $m_0$  represents the sky-only model corresponding to hypothesis (A), and  $m$  represents the model corresponding to hypothesis (B), based on Equation (2).

The likelihoods  $P(\rho|\text{sky}, m_0)$  and  $P(\rho|\hat{f}_{\lambda}, m)$  are given by:

$$\ln P(\rho_{\lambda}|\text{sky}, m_0) = -\frac{1}{2} \sum_i \frac{\rho_{\lambda i}^2}{\sigma_{\lambda i}^2} + \text{const.} \quad (9)$$

$$\ln P(\rho_{\lambda}|\hat{f}_{\lambda}, m) = -\frac{1}{2} \sum_i \frac{1}{\sigma_{\lambda i}^2} (\rho_{\lambda i} - \hat{f}_{\lambda} H_{\lambda i})^2 + \text{const.} \quad (10)$$

Assuming that we have no prior knowledge about the possible presence or absence of a source at  $\mathbf{s}$ , all of the other factors in (7) and (8) may be regarded as constants for present purposes, and we can thus express the probability ratio (source/sky) as:

$$\ln \frac{P(\hat{\mathbf{f}}|\rho, m)}{P(\text{sky}|\rho, m_0)} = \frac{1}{2} \sum_{\lambda} \hat{f}_{\lambda}^2 \sum_i \frac{H_{\lambda i}^2}{\sigma_{\lambda i}^2} + \text{const.} \quad (11)$$

Substituting for  $\hat{f}_{\lambda}$  using (6), we can express this probability ratio as:

$$\ln \frac{P(\hat{\mathbf{f}}|\rho, m)}{P(\text{sky}|\rho, m_0)} = \frac{1}{2} \phi(\mathbf{s})^2 + \text{const.} \quad (12)$$

where  $\phi(\mathbf{s})$  is defined as:

$$\phi(\mathbf{s}) = \left( \sum_{\lambda} \frac{1(\sum_i (\rho_{\lambda i}/\sigma_{\lambda i}^2) H_{\lambda}(\mathbf{r}_{\lambda i} - \mathbf{s}))^2}{\sum_i (1/\sigma_{\lambda i}^2) H_{\lambda}(\mathbf{r}_{\lambda i} - \mathbf{s})^2} \right)^{\frac{1}{2}} \quad (13)$$

in which we have replaced  $H_{\lambda i}$  by its more explicit form.

From (12), maxima in  $\phi(\mathbf{s})$  correspond to maxima in the (source/sky) probability ratio, and hence an image formed by calculating  $\phi(\mathbf{s})$  over a regular grid of positions,  $\mathbf{s}$ , would be a suitable basis for optimal source detection. It is apparent from (13) that such an image represents a quadrature sum of matched filters at the individual wavelengths, with appropriate normalization. The noise properties of such an image can be assessed by expressing  $\phi(\mathbf{s})$  in terms of the *a posteriori* variance of  $\hat{f}_{\lambda}$ , given by:

$$(\sigma_f^2)_{\lambda} = 1 / \sum_i \frac{H_{\lambda i}^2}{\sigma_{\lambda i}^2} \quad (14)$$

from which we obtain:

$$\phi(\mathbf{s}) = \left( \sum_{\lambda} \frac{\hat{f}_{\lambda}^2}{(\sigma_f^2)_{\lambda}} \right)^{\frac{1}{2}} \quad (15)$$

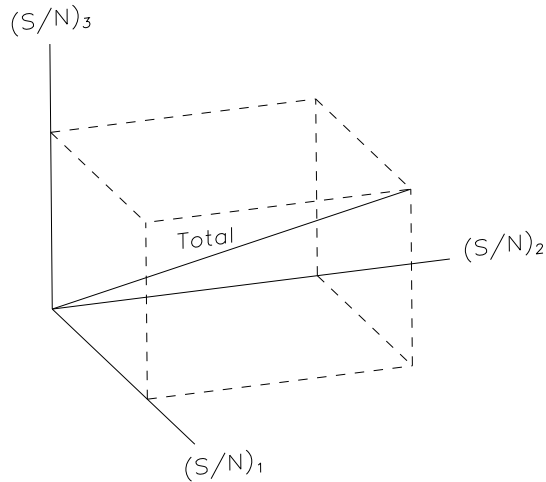


Figure 1: Combining matched filter images at several wavelengths. In this illustration, matched filter signals (in units of signal to noise ratio, SNR) from three separate bands are combined in quadrature to produce the total response.

It is readily shown, from (15), that the standard deviation of  $\phi(\mathbf{s})$  is unity, i.e.,  $\phi(\mathbf{s})$  itself is in units of standard deviations. Therefore, for a given detection threshold  $T_d$  [sigmas], the most likely locations of sources correspond to those for which  $\phi(\mathbf{s}) \geq T_d$ .

To summarize, the calculation of the optimal detection image from a set of multiwavelength observations involves simply the quadrature sum of the matched filter outputs (normalized in units of sigmas) at the individual wavelengths, as illustrated in Figure 1. Detection then consists of searching for local maxima which exceed a specified signal-to-noise threshold in this image.

This detection algorithm is similar to one proposed by Szalay et al. (1999), often referred to as the “chi squared” method. The central operation, in both cases, is a quadrature sum of matched filter images. An important difference between the two procedures, however, is the fact that in MDET we threshold the matched filter images at zero before squaring and combining, thus avoiding the contaminating effect of squared negative values in the image sum. This is a direct consequence of our prior information concerning the positivity of intensity, imposed via our Bayesian framework using Equation (5). It reduces the background noise on the combined image by a factor of  $\sqrt{2}$ , and therefore increases the sensitivity by the same factor.

### 3.3 The Effect of Cross-Band Source Blending

In the above derivation, the assumption was made that the instrumental responses of adjacent sources do not overlap. Although all matched filters are subject to this limitation, the situation may be more acute in the case of the multiband matched filter since images are being combined at multiple spatial resolutions. For the limited

range of spatial resolution in WISE (less than 3:1 ratio in FWHM between Bands 4 and 1) one would not expect any serious problems since, for example, closely-spaced (but distinct) peaks in the Band 1 image would normally produce local maxima in the combined image even if superposed on the wings of a broader Band 4 peak. However, if a source is present in Band 1 only, and a neighboring source is present in Band 4 only (or vice versa), the two sources could be blended into a single peak in the combined detection image even though they produced separate peaks in their respective single-band images. This situation is illustrated in Figure 2, which shows that for two sources separated by  $(FWHM_1 + FWHM_4)/2$  (where  $FWHM_1$  and  $FWHM_4$  represent the FWHMs of the point source responses at the respective bands, assumed to be Gaussian), then they become blended as a single peak when the strength ratio ( $SNR_1/SNR_4$ , i.e., the ratio of SNR values at the two bands) exceeds about 100. The behavior is further illustrated by Figure 3, which shows a plot of the critical separation as a function of strength ratio.

These effects can be overcome by supplementing the set of multiband detections with the results of single-band detections. By doing this, we maintain the increased sensitivity of multiband detection while not missing any detections due to cross-band blending effects.

## 4 IMPLEMENTATION

### 4.1 Procedure

The central operation in MDET is the calculation of the detection image, given by Equation (13). It is fortunate that the majority of the computations involved in this step (specifically, summations over the data pixels with weighting factors derived from the PSFs) are identical to those used in the calculation of the estimated sky brightness distribution at each band, performed by the WSDS image coadder (AWAIC; described in document WSDC D-D005). Therefore we can save a considerable amount of computation time by making appropriate use of the outputs of that module. Specifically, the calculation is based on an image set consisting of the following AWAIC products, one pair for each band to be incorporated:

**Coadded Image:**

$$\mathcal{I}_\lambda(\mathbf{s}) = \frac{\sum_i (\rho_{\lambda i} / \sigma_{\lambda i}^2) H_\lambda(\mathbf{r}_{\lambda i} - \mathbf{s})}{\sum_i (1 / \sigma_{\lambda i}^2) H_\lambda(\mathbf{r}_{\lambda i} - \mathbf{s})} \quad (16)$$

**Uncertainty Image:**

$$\mathcal{U}_\lambda(\mathbf{s}) = \frac{[\sum_i (1 / \sigma_{\lambda i}^2) H_\lambda(\mathbf{r}_{\lambda i} - \mathbf{s})^2]^{\frac{1}{2}}}{\sum_i (1 / \sigma_{\lambda i}^2) H_\lambda(\mathbf{r}_{\lambda i} - \mathbf{s})} \quad (17)$$

These two equations (16 and 17) correspond to (Eq. 9) and (Eq. 11), respectively, of the AWAIC document (WSDC D-D005).

Expressing the detection image,  $\phi(\mathbf{s})$ , in terms of the above two quantities using

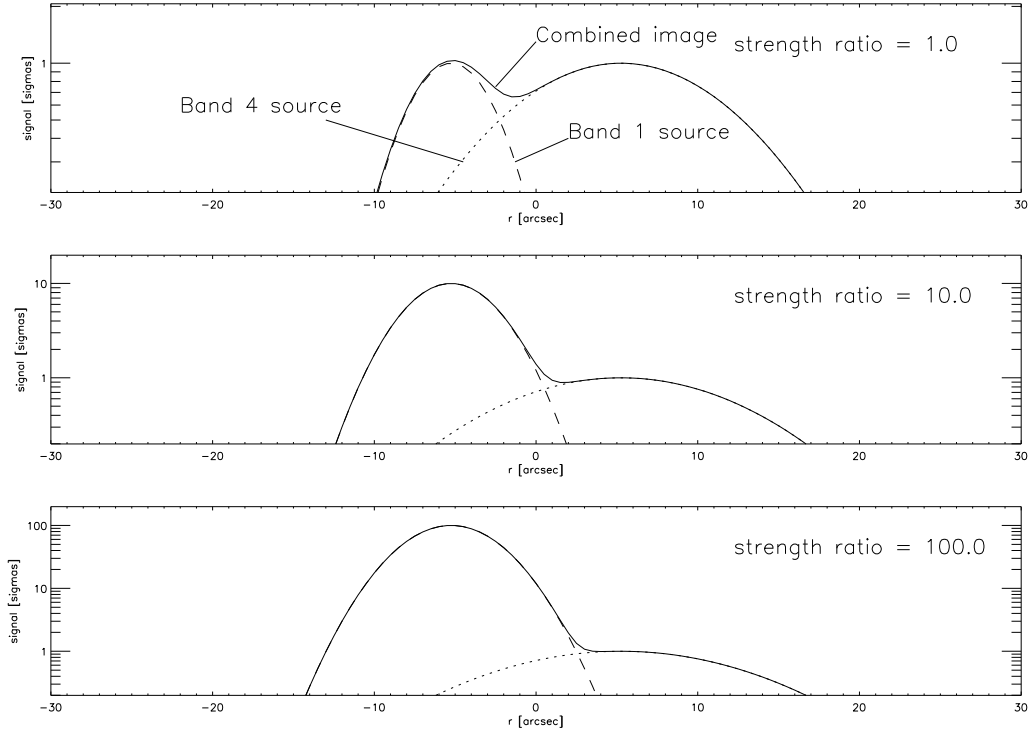


Figure 2: The effect of band-to-band source blending on the combined detection image. In this example, a Band 1-only source is separated from a Band 4-only source by a distance of  $10''.5$ . The sources are assumed to produce Gaussian-shaped responses on the single-band matched filter images (FWHM =  $6''$  and  $15''$  at Bands 1 and 4, respectively) as shown by the dashed and dotted lines. They combine to produce the multiband detection image as shown by the solid line in each plot. The three plots show the effect of varying the strength ratio of the two sources (defined as  $SNR_1/SNR_4$ ), and in particular that for this source separation, the two sources become blended as a single peak in the detection image (i.e., there is only one local maximum present) when the ratio of source SNRs exceeds about 100.

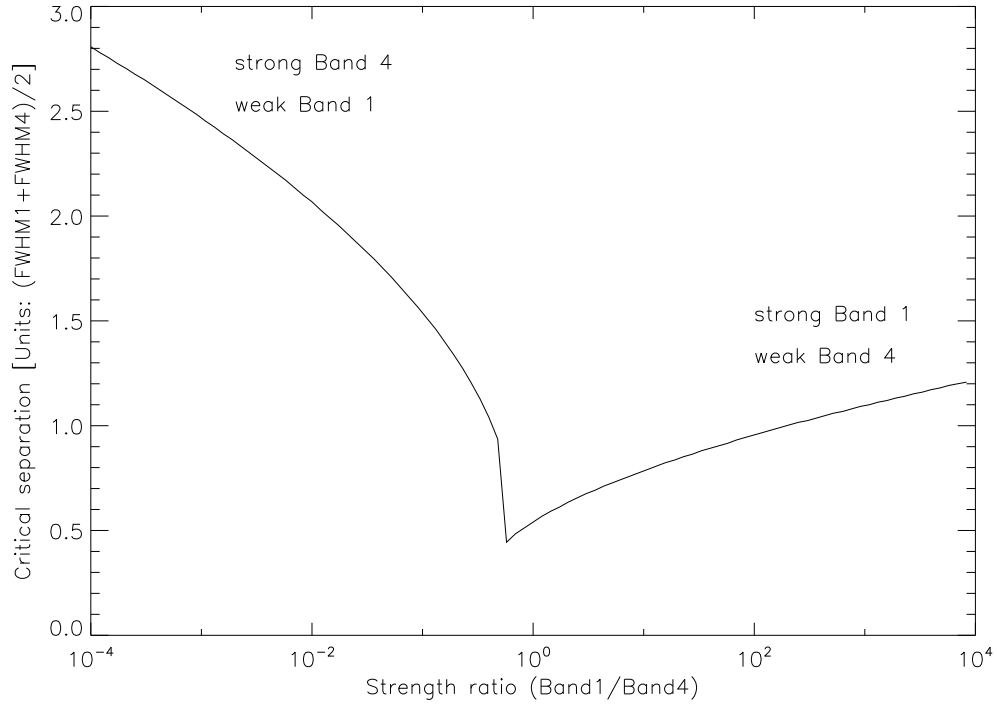


Figure 3: Critical separation as a function of source strength ratio for a pair of closely-spaced sources, one of which is seen in Band 1 only, and the other of which is seen in Band 4 only. The critical separation is in units of the scale length of  $10''.5$  (corresponding to  $(FWHM_1 + FWHM_2)/2$ ), and the strength ratio represents  $SNR_1/SNR_4$ , where  $SNR_1$  and  $SNR_4$  correspond to the signal to noise ratios of the sources in Bands 1 and 4, respectively. Sources separated by less than the critical value become blended as a single peak in the combined (multiband) detection image

Equation (13) we obtain:

$$\phi(\mathbf{s}) = \left( \sum_{\lambda} \left[ \frac{1(\mathcal{I}_{\lambda}(\mathbf{s}) - b_{\lambda}(\mathbf{s}))}{\mathcal{U}_{\lambda}(\mathbf{s})} \right]^2 \right)^{\frac{1}{2}} \quad (18)$$

where  $b_{\lambda}(\mathbf{s})$  represents the slowly-varying sky background, estimated using median filtering of the coadded image with a specified window size,  $w_{\lambda}$ , chosen to be somewhat smaller than the assumed (*a priori*) minimum scale of sky background variations.

So the multiband detection procedure is:

1. Estimate a slowly-varying sky background at each wavelength by median filtering the coadded images with an appropriately-sized window.
2. Subtract the estimated background from each coadded image.
3. Calculate the optimal matched filter at each wavelength (represented by an individual term in square brackets in Equation (18)).
4. Zero out negative pixel values in each of the single-band matched filter images.
5. Combine the resulting single-band images in quadrature to produce a detection image in units of sigma (the local standard deviation of noise).
6. Locate all local maxima in the detection image, to an accuracy corresponding to the pixel size of the coadded image grid.
7. List the positions (RA and Dec) and strengths (i.e., SNR values) of all local maxima which exceed the desired detection threshold in sigmas, in order of decreasing SNR.
8. Repeat the detection procedure for each band individually and supplement the multiband source list with any single-band detections that were missed in the multiband step. The criterion for the inclusion of a single-band detection is that the distance between it and the nearest source on the multiband source list should exceed a critical distance,  $r_{\text{crit}}$ . The latter corresponds to the minimum distance between distinguishable peaks on the matched filter image for the band in question, for which an appropriate value is 1.6 times the FWHM of the PSF in that band.

## 4.2 Allowance for confusion

In regions of high source density, such as the Galactic Plane, the effects of unresolved background sources may be regarded as an additional stochastic component in the measurement model for our sources of interest (the latter being defined as point sources spatially resolvable either directly by the measurement system, or by subsequent processing). This stochastic component, referred to as “confusion noise” should

be taken account of during the setting of the detection threshold in order to avoid the attempted extraction of large numbers of non-deblendable sources. To facilitate this, we can express the coadded image at a given wavelength as:

$$\mathcal{I}(\mathbf{s}) = \kappa(\mathbf{s}) * [B(\mathbf{s}) + \delta B(\mathbf{s})] + b(\mathbf{s}) + \nu(\mathbf{s}) \quad (19)$$

where  $B(\mathbf{s})$  represents the sky brightness distribution due to the discrete sources of interest,  $\delta B(\mathbf{s})$  represents the spatial brightness fluctuations about the mean local background level due to confusing background sources,  $\nu(\mathbf{s})$  represents measurement noise,  $\kappa(\mathbf{s})$  represents the overall convolution kernel resulting from the measurement system and the coadding process, and  $*$  denotes convolution. The subscript  $\lambda$  has been dropped for clarity.

Expanding (19) we obtain:

$$\mathcal{I}(\mathbf{s}) = \kappa(\mathbf{s}) * B(\mathbf{s}) + b(\mathbf{s}) + \mu(\mathbf{s}) \quad (20)$$

where

$$\mu(\mathbf{s}) = \kappa(\mathbf{s}) * \delta B(\mathbf{s}) + \nu(\mathbf{s}) \quad (21)$$

Since the confusion noise is statistically independent of the measurement noise, we can express the covariance of  $\mu$  as the sum of the covariances of the two terms on the right hand side of (21), i.e.,

$$C_{\mu}(\mathbf{s}, \mathbf{s}') = C_{\text{conf}}(\mathbf{s}, \mathbf{s}') + C_{\nu}(\mathbf{s}, \mathbf{s}') \quad (22)$$

where  $C_{\text{conf}}$  represents the covariance of the smoothed brightness distribution,  $\kappa * \delta B$ .

In the absence of confusion, the detection threshold is derived from the coadd uncertainty image,  $\mathcal{U}(\mathbf{s})$ , which corresponds to the square root of the diagonal elements of  $C_{\nu}$ . In the presence of confusion, however, Equation (22) indicates that we should modify this uncertainty by adding the diagonal elements of  $C_{\text{conf}}$  to those of  $C_{\nu}$ . The former correspond to the squares of the standard deviations of confusion noise in the coadded image.

Thus to take account of confusion noise in the detection process we simply need to add, in quadrature, a confusion term to  $\mathcal{U}$  in Equation (18). An appropriate value can be obtained by modeling the distribution of sky brightness values in terms of an equivalent Gaussian (motivated by the Central Limit Theorem, assuming a sufficiently large number of unresolved background sources is being averaged in the beam) upon which is superposed a tail which includes our sources of interest. Specifically, we take half the difference between the 15.87% and 84.13% quantiles of the brightness histogram as a measure of the standard deviation and subtract, in quadrature, the contribution of measurement noise. This is similar to the technique used successfully for setting the detection threshold in 2MASS, whereby the estimate was based on the difference between the 32.22% and 50 % quantiles of the sky brightness histogram (Cutri et al. 2003).

Naturally, this allowance for confusion increases the image sigma, so that if we regard the detection threshold as being constant in terms of SNR, the implication is that we are raising the flux density limit in confused regions.

### 4.3 Inputs

Although the focal-plane image data, the PSF, and the noise model parameters represent the fundamental information on which the detection image is based, this information is all encoded in the coadder output. The only inputs required for the detector are thus:

1. Coadded image at each band.
2. Corresponding set of uncertainty images.
3. Detection threshold in sigmas.
4. Width of median filtering window [arcmin] at each band, for background estimation.
5. Width [arcmin] of window used for estimating the confusion noise term.

### 4.4 Outputs

The output consists of:

1. Source list.
2. Median-filtered background image for subsequent use in source characterization (FITS format).

The source list is a text file, each line of which contains the following information:

1. Sequential number of source (integer); the ordering is in decreasing SNR.
2. RA [deg] (double precision real)
3. Dec [deg] (double precision real)
4. Source strength [sigmas] (real)

The reason that the positions are quoted in RA and Dec rather than pixel coordinates is that, in general, the detection image represents a combination of images from different bands and/or dithered framesets, with frame-to-frame registration based on the WCS information in the FITS headers.

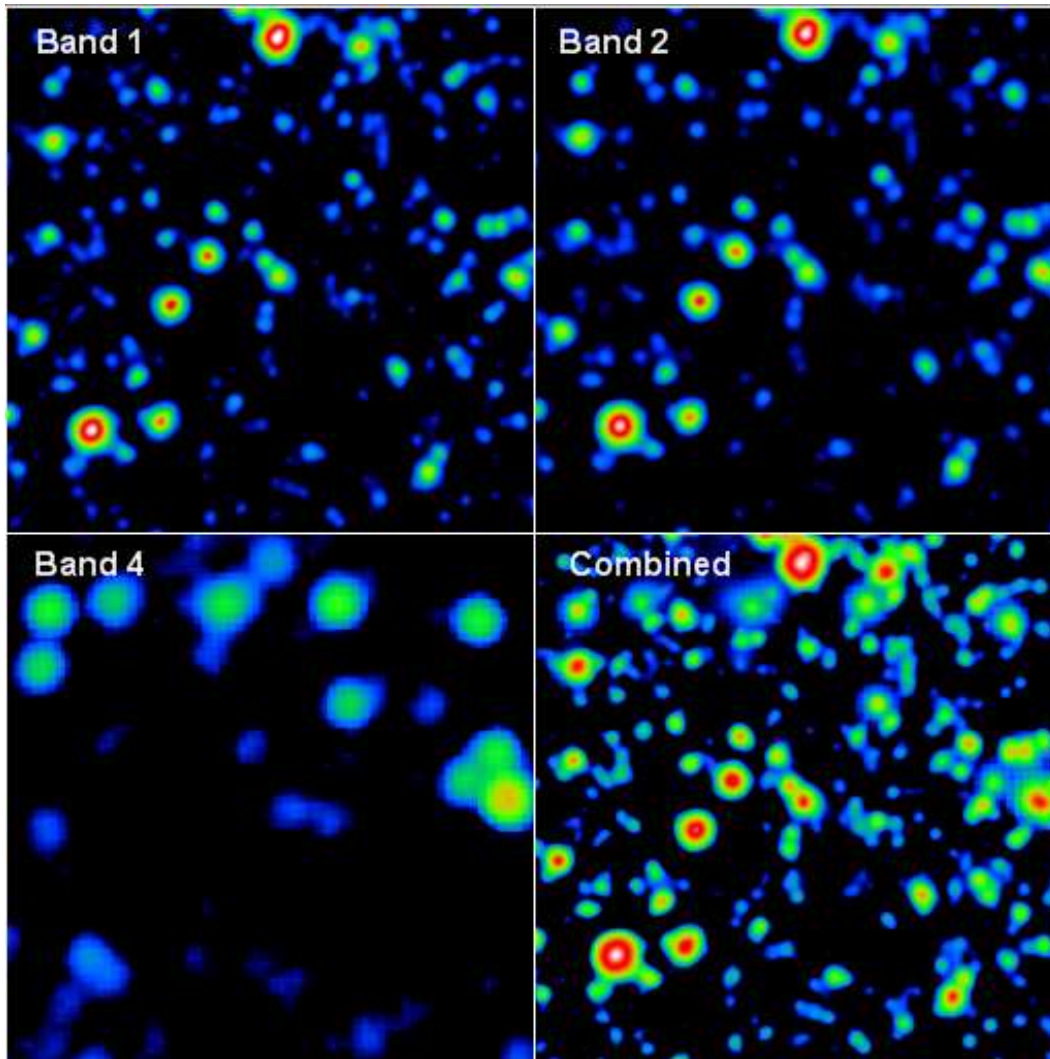


Figure 4: Example of a multiwavelength matched filter calculation based on a simulation of the Galactic Center using realistic values for WISE instrumental parameters. Three of the four panels show the central  $5.9 \times 5.9$  portion of the simulated focal-plane images in bands 1, 2, and 4 (after dark subtraction, flat fielding, distortion correction and interpolation to a finer grid using the AWAIC module); the fourth image (“Combined”) shows the corresponding detection image produced by MDET, representing an optimal combination of the focal-plane images at bands 1, 2, 3, and 4. For all four panels, the intensity scale is logarithmic, covering the range  $(10^0-10^3)\sigma$ , where  $\sigma$  represents the noise level for the particular image.

## 5 TESTING

MDET has been coded in Fortran and tested with synthetic data. A particularly useful example is a simulation of the Galactic Center region, using one of the framesets (4 focal-plane images, one for each band) generated by N. Wright (dataset designation: 10076220928). The 4 focal-plane images were combined to produce a detection image with a field of view of  $47' \times 47'$ , a  $5.9 \times 5.9$  subfield of which is shown in Figure 4. This is a particularly crowded field, and provides a good test of a number of aspects of our detection scheme.

One important test is to compare the results obtained using multiband detection with those obtained by doing the detection one band at a time followed by bandmerging. For this purpose, we conducted an initial test in which we excluded Step #8 of the MDET implementation procedure discussed in Section 4, i.e. the multiband detection list was not supplemented with the results of single-band detections. The following results were then obtained:

Table 1: Summary of results.

Band:	Number of candidate detections:	
	threshold = $5\sigma$	threshold = $3\sigma$
1	972	2080
2	254	533
3	35	74
4	11	28
Result of merging single-band detections:	978	2093
Result of multiband detection:	1107	2315
# multiband candidates not in merged list:	138	243
# merged candidates not in multiband list:	9	21
# blended sources missed by multiband detector:	5	12
# spurious bandmerged detections:	4	9

It is apparent that significantly more sources were detected using the multiband detector (MDET) than with single-band detection followed by bandmerging. This behavior is expected due to the  $\sqrt{N}$  effect resulting from combining the images. To be more specific, multiband detection found about 10% more sources than did the single-band detection. By contrast, only about 0.5% of apparently genuine sources found by single-band detection were missed by MDET. Examination of the data showed that they were missed as a result of the cross-band confusion effect illustrated in Figure 2. This underscores the necessity for inclusion of Step #8 in the implementation procedure. Using the full algorithm (i.e., including Step #8) we verified that all of the sources previously missed by the multiband detector were then recovered.

MDET has now been tested extensively in the source extraction pipeline using further WISE data simulations generated by N. Wright, and the results compared with the corresponding truth tables. The tests included all cases applicable to WISE,

i.e., (1) single-band single-frame, (2) single-frameset with all 4 bands, and (3) the full multiband, multiframe case. In each case, using a detection threshold of  $15\sigma$  for case (1) and  $3.8\sigma$  for the other two cases, all expected sources are recovered. These tests are ongoing, and this document will be updated accordingly.

## 6 REMAINING ISSUES

Some additional issues to be addressed in future testing are:

1. What are the optimal window sizes for slowly-varying background estimation and confusion estimation?
2. What will be the behavior of the detector in the vicinity of a large extended object such as M31, or in the vicinity of nebulosity? Should the window sizes be made adaptive for such situations?
3. How many spurious detections occur in the vicinity of a strong saturated source?
4. Quantify the possible effects of pixel-to-pixel and band-to-band correlations of detector noise.

## 7 SUMMARY

MDET performs the source detection step associated with each of the three stages of source extraction during pipeline processing (single frame, single-epoch 4-band frameset, and final coadd stage). With the exception of the first (single-frame) stage, the detection (followed by source characterization) is done at multiple bands simultaneously. Based on the usual assumptions for source detection in astronomical images (non-blended sources in the presence of additive Gaussian noise), the optimal *multiband* detector represents a quadrature sum of the matched filter images in the individual bands. This image is then thresholded at the appropriate SNR for detection purposes. The output is a list of source candidates to be fed to the photometry module for the subsequent source characterization. Our tests support the expectation that the multiband detector provides increased sensitivity over the traditional technique of single-band detection + bandmerging.

## 8 ACKNOWLEDGEMENTS

I thank Roc Cutri for guidance with this work, and Frank Masci and Tom Jarrett for helpful discussions.

## 9 REFERENCES

- Bertin, E. & Arnouts, S. 1996, *A&AS*, 117, 393
- Cutri, R. et al. 2003, “Explanatory Supplement to the 2MASS All Sky Data Release and Extended Mission Products”  
<http://www.ipac.caltech.edu/2mass/releases/allsky/doc/explsup.html>
- Stetson, P. B. 1987, *PASP*, 99, 191
- Szalay, A. S., Connolly, A. J. & Szokoly, G. P. 1999, 117, 68